Chemical Engineering Journal 457 (2023) 141282

Contents lists available at ScienceDirect

Chemical Engineering Journal

journal homepage: www.elsevier.com/locate/cej

Super-tough, self-sensing and shape-programmable polymers via topological structure crosslinking networks

Lan Luo [a], Fenghua Zhang [a,*], Yanju Liu [b], Jinsong Leng [a,*]

[a] Centre for Composite Materials and Structures, Harbin Institute of Technology (HIT), Harbin 150080, People's Republic of China
[b] Department of Astronautical Science and Mechanics, Harbin Institute of Technology (HIT), Harbin 150001, People's Republic of China

ARTICLE INFO

Keywords:
Topological structure
Super-tough
High-temperature resistance
Triple-shape memory
Molecular simulation

ABSTRACT

Shape-memory polymers (SMPs) are smart materials capable of deforming actively under external excitation. Owing to their characteristics, including variable stiffness, programmable deformation, composability, and self-sensing, and its behavior is similar to the intelligent reflection of life, these materials are highly valuable for applications in many fields. We have developed a molecular engineering strategy based on topological cross-linking networks, which form hydrogen bonds, hyperbranching, ring network structure, etc. to obtain shape memory epoxy resin (SMEP) with super toughness, high-temperature resistance and triple shape memory effect (TSME). Additionally, the internal relationship between the molecular network structure and material performance is simulated by molecular dynamics. It has super toughness (1288 %) and high impact energy (216 MJ/m^3) above its transition temperature, breaking through the previously reported thermosetting resin. Importantly, the developed SMPs system exhibited outstanding fatigue resistance and was successfully loaded repeatedly for more than 100 cycles. Finally, the intramolecular cyclization effect led to the generation of different linked structures in situ, which endowed SMEP with TSME, thereby rendering such materials potentially applicable in engineering fields, such as aerospace, smart furniture, and soft robotics.

1. Introduction

Shape-memory polymers (SMPs) and their composites are an emerging class of functional macromolecular materials capable of self-sensing from changes in the external environment, and they respond to such changes by recovering to a predetermined state [1–5]. SMPs that respond to different stimuli (e.g., heat, light, electricity, and magnetism) constitute an important material basis for realizing smart changeable structures [4,6,7]. Objects produced from SMPs are no longer static and inanimate; instead, they feature forms and structures that change dynamically over time. Owing to their characteristics (e.g., variable stiffness and programmable and large deformation), SMPs and their composites have been extensively developed to provide materials for application in the fields of aerospace engineering, biomedicine, flexible electronics, and soft robotics [8–15]. Specifically, as an important class of resins, thermosetting shape-memory epoxy polymers (SMEPs) are known for their excellent chemical stabilities and mechanical properties [16].

However, despite their numerous advantages, the applications of SMEPs in the aerospace industry are limited because of their poor high-temperature resistance and brittleness after curing. Additionally, several other issues must be urgently addressed for facilitating their widespread applications. For example, owing to the high internal stresses exhibited by epoxy resins, the 3D network structures of thermosetting resins formed after curing are disadvantageous because of their low degrees of potential deformation. Therefore, optimizing the performances of SMEPs in terms of toughness, high-temperature resistance, requires investigation. Xie et al. reported a strain of 212 % at the glass-transition temperature (T_g) of SMEP comprising a two-component epoxy–amine curing system [17]. Although several SMPs exhibit integrated deformations and their load-bearing capacity have been developed and preliminarily examined for applications in the aerospace field [18–22]. However, because their constituent epoxy resins face extreme challenges when operating at temperatures above 200 °C, and therefore, these SMPs cannot meet the high-temperature demands of the aerospace industry. Therefore, it is necessary to develop SMPs capable of withstanding high temperatures [23]. Additionally, triple-SMEPs must be capable of undergoing multi-stage deformation. For example, in the Starlink satellite-based internet connectivity program, to reduce drag and level the satellites, the solar panels were not initially fully unfolded,

* Corresponding authors.
E-mail addresses: fhzhang_hit@163.com (F. Zhang), lengjs@hit.edu.cn (J. Leng).

https://doi.org/10.1016/j.cej.2023.141282
Received 29 October 2022; Received in revised form 18 December 2022; Accepted 1 January 2023
Available online 2 January 2023

and they are only fully unfolded in operating mode. Therefore, the solar panels changed between two attitudes. However, multifunctional SMEPs with multi-response, multi-shape, and bidirectional shape memory properties are receiving growing attention to generating new materials that meet various demands. The triple-shape SMP (TSMP) based on epoxy resin can be realized in the following ways. The polymer compound generates SMP hybrid, the two internal networks are semi-interpenetrating networks and full interpenetrating networks. On the other hand, two resin layers with different T_g are laminated to obtain TSMP in the traditional sense of the composite system. The key to a triple-shape SMP is as follows: having a "wide" T_g range or generating a common network with two "transitions", on the other hand, to combine two different T_g-EP layer systems [22]. Karger et al. prepared an EP/polycaprolactone (PCL) triple-shape memory effect (TSME) and designed its temporary shapes according to the T_g of the EP and the melting temperature (T_m) of PCL [24,25]. Furthermore, Xie et al. conducted an in-depth investigation of TSME, combining two SMEPs with different T_g values to form a bilayer polymer and adjusting the fixed shape of the TSME by altering the ratio of the two SMEPs [26]. In our previous study, the SMEP network structure was adjusted to alter its glass-transition range [27].

Herein, we report the conversion of a crosslinked epoxy resin model into a visually discernible network structure using the coarse-graining method combined with the all-atom method. Additionally, molecular dynamics (MD) simulations are used to simulate topological network structure and estimate the material properties. Specifically, a synergistic strategy involving flexible chains and hydrogen bonds is applied to construct a Bi-EP system with high robustness (owing to the dense interbond hydrogen bonds), and a network structure possessing exceptional tensile properties and super-toughness. The Tri-SMEP system is prepared using tri-functional monomers with high T_g, which is expected to surpass the previous application limit of 200 °C. This should be possible because of the presence of highly functional epoxy monomers that lead to the formation of a tightly arranged network. Tetra-EP system formed by tetrafunctional epoxy monomer has intramolecular cyclization due to steric hindrance effect, which reveals for the first time the triple-shape memory mechanism of cross-linked network in situ formation. Our work represents a major leap forward in expanding the mechanical and thermal properties of epoxy resins and provides the foundation for overcoming performance deficiencies through smart material design. Therefore, the developed series of high-performance and self-sensing SMEPs are expected to play practical roles in different engineering fields.

2. Materials and methods

2.1. Materials

Bisphenol A glycidyl ether (DGEBA), Triglycidyl p-aminophenol ether (TGPA), Tetraepoxypropyl-4,4′-diaminodiphenylmethane ether (TGME). Epichlorohydrin, ethylene glycol, diaminodiphenylmethane, acetone, toluene, Chain extenders include ethylene glycol diglycidyl ether (HDE), 1,4-butanediol glycidyl ether (BDDE), and 1,6-hexanediol diglycidyl ether (EGDE). Curing agents include p-phenylenediamine (PDA) and Diethyltoluenediamine (DETDA).

2.2. Synthesis of TGME

Epichlorohydrin, ethylene glycol and water were heated to 50 °C under stirring, and diaminodiphenylmethane was added over 3 h. The reaction mixture was then heated to 60 °C, and acetone (16 mL) was added. Under stirring, the reaction was allowed to continue for 10 h, and subsequently, a further portion of acetone was added to yield a transparent solution. Thereafter, the reaction mixture was cooled, and a liquid alkali was slowly added to promote the cyclization reaction. After stirring for 40–80 min, toluene (50 mL) was added, and the mixture was stirred for 15 min and subsequently allowed to stand for stratification. The solvent was then removed under reduced pressure conditions and filtered while hot to obtain TGME as a pale-yellow product. The ^1H nuclear magnetic resonance spectrum of the resulting material is shown in Fig. S1.

2.3. Fabrication of SMEPs

The chemical structure of all epoxy monomers, chain extenders, and crosslinkers is shown in Fig. S2. To prepare the Bi-EP system, the crosslinking reactions of chain extenders (HDE, BDDE, EGDE) of different chain lengths were performed in the presence of Bi-EP and curing agents respectively. Curing was then conducted for 2 h at 80 °C and for 8 h at 140 °C, and after subsequent cooling, the Bi/EP, HDE/EP, BDDE/EP, and EGDE/EP systems were obtained. The Tri-EP system was obtained by the reaction of TGPA and the DETDA. According to the crosslinking density of 70 %, 80 %, 90 % and 100 %, Tri/EP-1, Tri/EP-2, Tri/EP-3 and Tri/EP-4 are obtained respectively. In the system Tetra-EP, the obtained TGME is subjected to crosslinking reaction with curing agent DETDA in different proportions. According to the cross-linking density of 70 %, 80 %, 90 %, and 100 %, the samples Tetra/EP-1, Tetra/EP-2, Tetra EP-3, and Tetra/EP-4 are obtained respectively.

2.4. Chemical and structural characterization

Fourier transform infrared (FT-IR) spectroscopy was performed on a Nicolet-Nexus-670 FT-IR spectrometer using the KBr disk method. The spectra were recorded between 400 and 4000 cm^{-1} to evaluate the molecular structure of different epoxy curing systems. The T_g values of the samples were determined by differential scanning calorimetry (DSC) upon scanning from 25 to 300 °C at a rate of 5 °C/min in a nitrogen atmosphere. To avoid the influence of the material thermal history, the second heating cycle was used for the measurement of the T_g values. Thermogravimetric analysis (TGA) was performed for thermal stability testing. Specifically, the samples were heated from 25 to 800 °C at a rate of 10 °C/min in a ceramic crucible in a nitrogen atmosphere. The cross-link density was measured by swelling method [28]. The square piece samples were placed in a 25 mL acetone solvent grinding bottle, tightly capped, and removed after 48 h of swelling. Absorb and weigh the surface solvent, and then place it in an oven at 100 °C for 12 h, and then weigh it to obtain the cross-linking density. See Table 1 for the test results.

Tensile tests were conducted using a Zwick/Roell Universal Testing System. For this purpose, dumbbell-shaped samples measuring 2–3 mm in thickness and 8 mm in width were employed. Tensile tests were performed at room temperature and at a range of other temperatures using equal tensile and unloading rates of 2 mm/min, wherein a 50 % strain was employed. This cycle was repeated until the breakage of specimen. Dynamic mechanical thermal analysis (DMA) investigated the thermo-mechanical properties of the samples. The samples were heated from 25 to 30 °C at a rate of 3 °C/min using the multi-frequency strain mode with a constant applied frequency of 1 Hz. The shape memory behavior was tested by bending, twisting, and stretching the material under the application of an external force. After heating the specimens to their corresponding T_g values, the softened samples were shaped and then rapidly cooled to obtain the desired temporary shape.

3. Results and discussion

3.1. Molecular dynamics simulation

MD simulations allow the investigation of microscopic properties of materials to be investigated at a molecular level. As EPs contain multiple crosslinked reactive sites, the experimental study of their network structures after crosslinking is difficult. Instead, their crosslinked network properties can be theoretically elucidated using MD simulations

with the help of material studio software to provide theoretical guidance for the experimental study. Therefore, considering the formation of crosslinked epoxy networks in our current system, the reaction of the epoxy group was initially investigated via all-atom MD simulations [29,30]. Molecular system models with identical dimensions but different ratios were constructed and simulated using the all-atom method. For this purpose, the resin and curing agent molecules were evenly mixed in the desired proportion to match experimental conditions. The ring-opening hydrogenation of the epoxy bond was then simulated to form accessible reaction sites, from which the active hydrogen atoms were removed by the curing agent. Subsequently, the crosslinking of the molecular systems was simulated to generate network structures; these structures were simplified by coarse-graining and were then cleaned (Fig. 1a). As shown in Fig. 1b, MD simulations were used to calculate and simulate the free volume of different systems, wherein the purple regions indicate the free volumes. The results indicated that the Bi-EP system possesses the largest free volume, and as the flexible chain grows in length, the free volume increases. Although the Tri-EP system exhibited the smallest free volume in terms of percentage (up to 10.6 %), it possessed the highest crosslinked network density. This was because steric hindrance prevents the occurrence of intramolecular cyclization, which is described in section 3.3.

The existence of multiple reaction sites of DETDA provides more possibilities for the cross-linking network structure. When DETDA with different reactivity is taken as the research object, each DETDA molecule can connect up to 4 bonds. However, due to the steric hindrance effect and segment motion, many DETDA molecules cannot be cross-linked by the maximum number of connections. Fig. 1c shows the free volumes calculated for different systems. Bi/EP, Tri/EP-1 and Tetra/EP-1 samples with the same degree of crosslinking were selected to calculate the concentration change and radial distribution function (RDF). Fig. 1d shows the variation in the concentration within each resin system (as simulated using the Forcite module), which reflects the uniformity of dispersion in each direction. The resin in each crosslinked system was distributed around 1, suggesting that the molecules in the crosslinked network were uniformly distributed in all directions. Additionally, Fig. 1e shows a graph of intermolecular radial distribution function (RDF) of each system. Wherein the degree of molecular stacking in each system ultimately tends to 1. Furthermore, higher RDF values are associated with more compact molecular stacking, and therefore, the Tri-EP system possesses the highest value, followed by the Tetra-EP system, these results are consistent with the trend of Young's modulus (Fig. S3).

3.2. Properties of the polyfunctional-SMEPs

Different topological cross-linked network structures formed by the ring-opening reactions of polyfunctional epoxy monomers with the active hydrogen atoms of the polyamine curing agents are presented in Fig. 2a. All infrared test curves are homogenized and analyzed, as shown

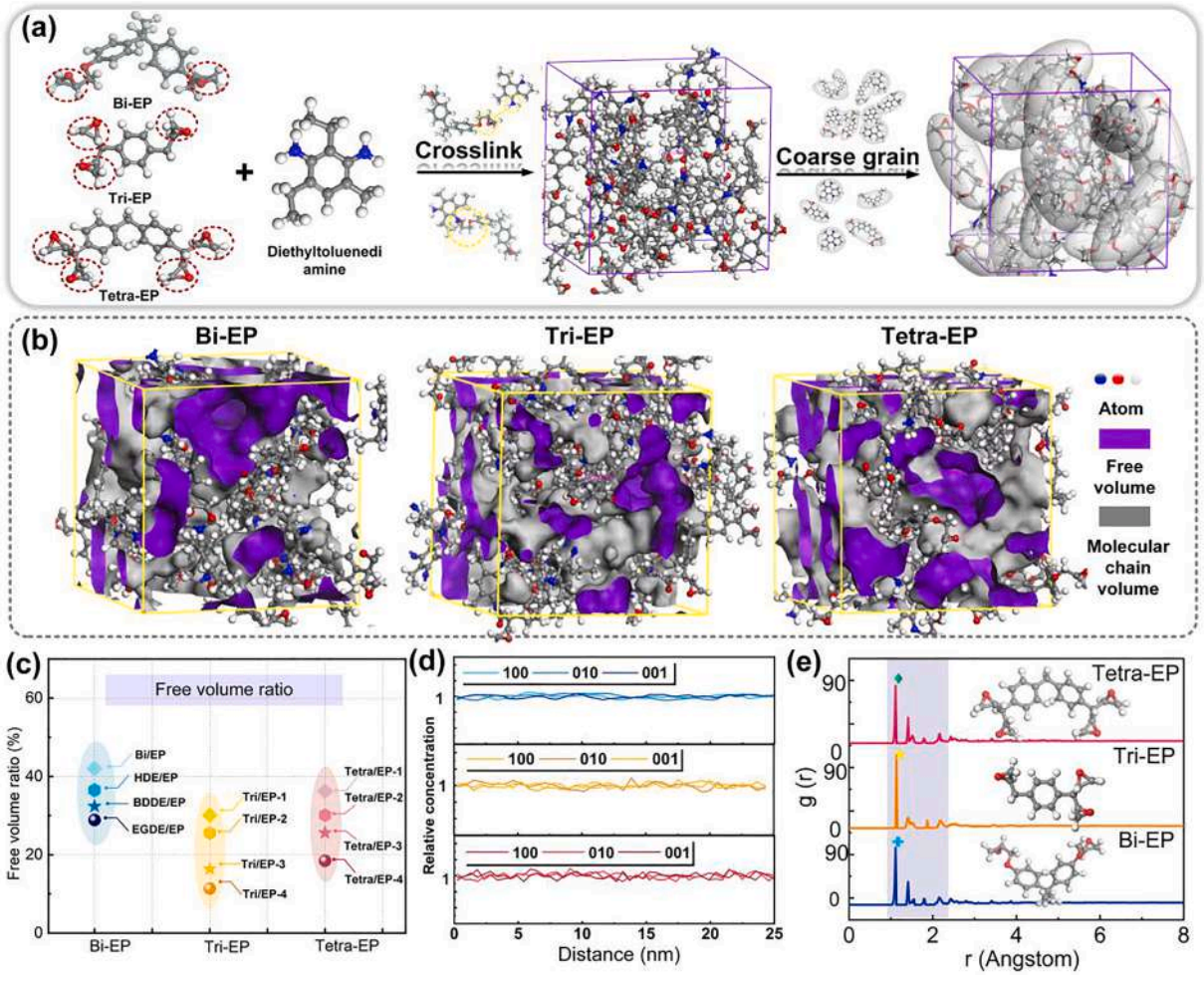

Fig. 1. Molecular dynamics simulation results of SMEPs with different crosslinked network structures. (a) Schematic diagram of molecular dynamics simulation of resin network crosslinking and coarse-graining process. (b) Schematic diagram of the free volume of crosslinked structures of different systems calculated by molecular dynamics. (c) Free volume results from molecular dynamics simulation calculations for all samples. (d) Molecular dynamics calculates the concentration distribution of the different systems. (e) Intermolecular radial distribution function curves of all systems.

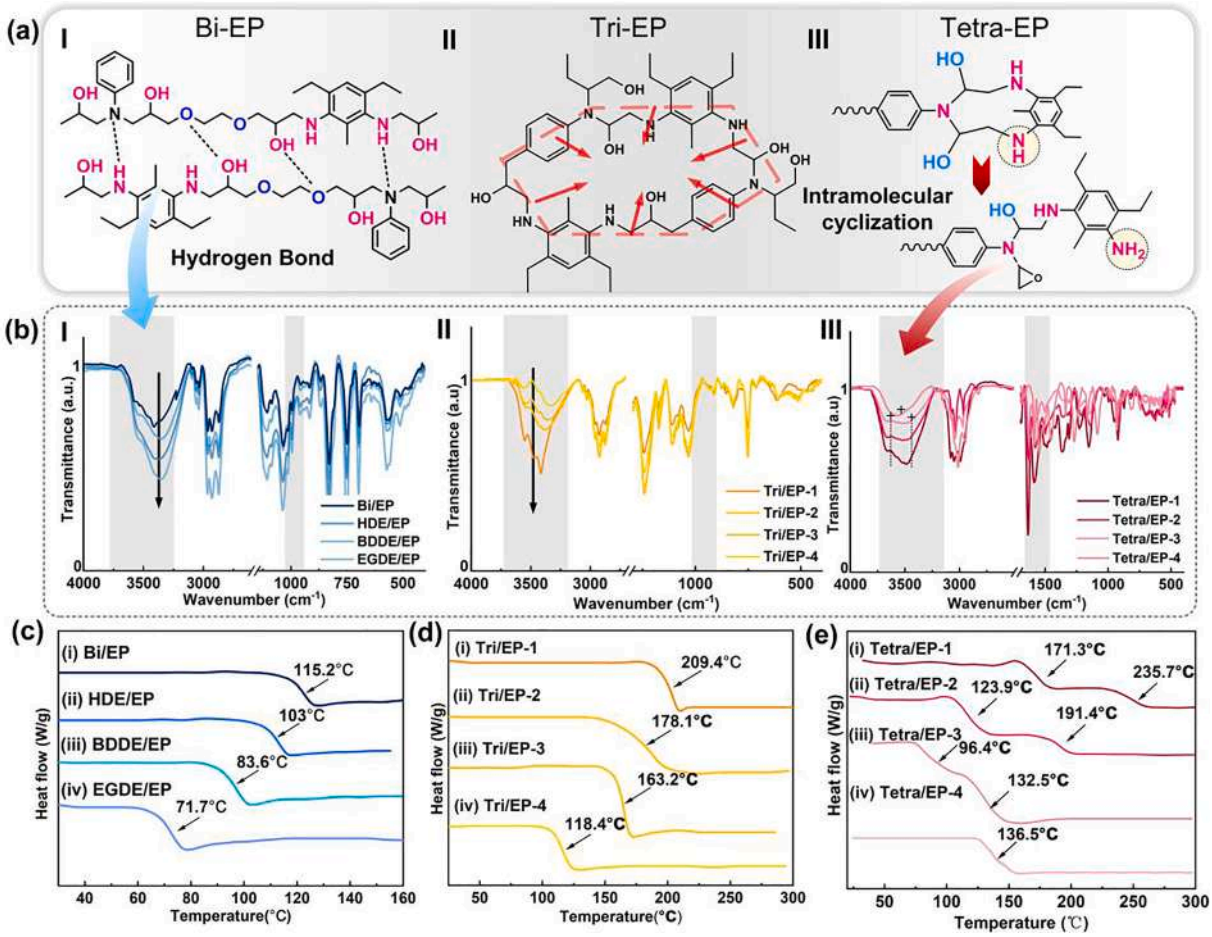

Fig. 2. Characterization of chemical properties of SMEPs with different crosslinked network structures. (a) Crosslinking reaction of epoxy monomers with different functionalities. (b) FTIR spectra of all systems. (c) DSC curves of the Bi-EP system. (d)DSC curves of the Tri-EP system. (e)DSC curves of the Tetra-EP system.

in Fig. 2(b). Additionally, the FT-IR analysis of the Bi-EP system indicates the presence of symmetric and antisymmetric methylene stretching vibrations of methylenes at 2926.6 cm^{-1} and 2857.5 cm^{-1}, respectively, which suggest the successful introduction of flexible alkyl flexible chains. Furthermore, hydrogen bonds are formed between the main chain ether bonds and the hydroxyl group formed via the curing reaction. As the number of hydrogen bonds and flexible chains increased, the characteristic IR peaks of the alkyl groups and ether bonds strengthened, as observed in Fig. 2b. The analysis of region II (see Fig. 2b) reveals that the hydroxyl peaks become increasingly pronounced as the degree of crosslinking increased, suggesting that an increasing number of epoxy groups are cured through ring-opening polymerization process, followed by the gradual disappearance of the peaks. This indicates that the Tri/EP system transformed more saturated DETDA molecules than the other systems. Analysis of the FTIR spectrum of the Tetra-EP system revealed exceptionally strong peaks corresponding to the presence of benzene rings (owing to the increased degree of crosslinking) and the disappearance of epoxy groups observed for the Tetra/EP-1. As the degree of steric hindrance is reduced as the crosslinking network density decreases, and as the intramolecular cyclization side reaction becomes less frequent, a larger number of epoxy groups is effectively introduced into the crosslinking system. Bellenger et al. revealed the process in which the amino group on the curing agent changes into a secondary amine with a gradual reaction during the epoxy curing reaction. The variations of their relative importance with the amine structure and the crosslink density are discussed in terms of steric configurations [31,32]. Since the epoxy group has reacted with the amino group in the curing agent, the adjacent epoxy group cannot continue to open the ring. More free primary amine groups are produced, and the V_{NH} peak will move to 3350 ~ 3310 due to association. Therefore, from region III of Fig. 2b, the two primary amine peaks gradually convert into a single secondary amine peak. However, samples with reduced crosslinking degree are prone to the intramolecular cyclization side reaction, which leads to a higher degree of steric hindrance owing to the short distance between the two epoxy groups being too close [29,33].

Fig. 2c shows the DSC test results for all the samples. Specifically, as the flexible chains of glycidyl ether become longer, the T_g of the Bi-EP system gradually shifts to the low-temperature range, decreasing from 115.2 °C to 71.7 °C. Additionally, as the density of the crosslinked network density increases in the Tri-EP system, the T_g increases to 209.4 °C (Fig. 2d). As trifunctional monomers exhibit negligible steric hindrances and are not prone to the cyclization side reaction, the resulting cured products possess a higher crosslinking density, this is consistent with the trend observed in the MD simulation [34]. As shown in Fig. 2e, except for Tetra/EP-4, all samples exhibit two-step peaks, thereby suggesting the existence of two T_g values. In the case of the Tetra/EP-4 specimen, the single Tg value is extremely high, and this finding is corroborated by the DMA test curves (Fig. 3). From the local amplification of the TGA curve shown in Fig. S4, thermal decomposition begins at 355 °C, leaving ~10 % carbon residue at 500 °C. Based on the thermal decomposition begins at 355 °C. From the thermal decomposition temperature of each sample, it can be concluded that the lower the degree of crosslinking, the earlier the thermal decomposition occurs, such as Tri/EP-4 and Tetra/EP-4. Specifically, at 500 °C, the residual carbon content of Tetra/EP-1 is ~40 %, and the thermal decomposition

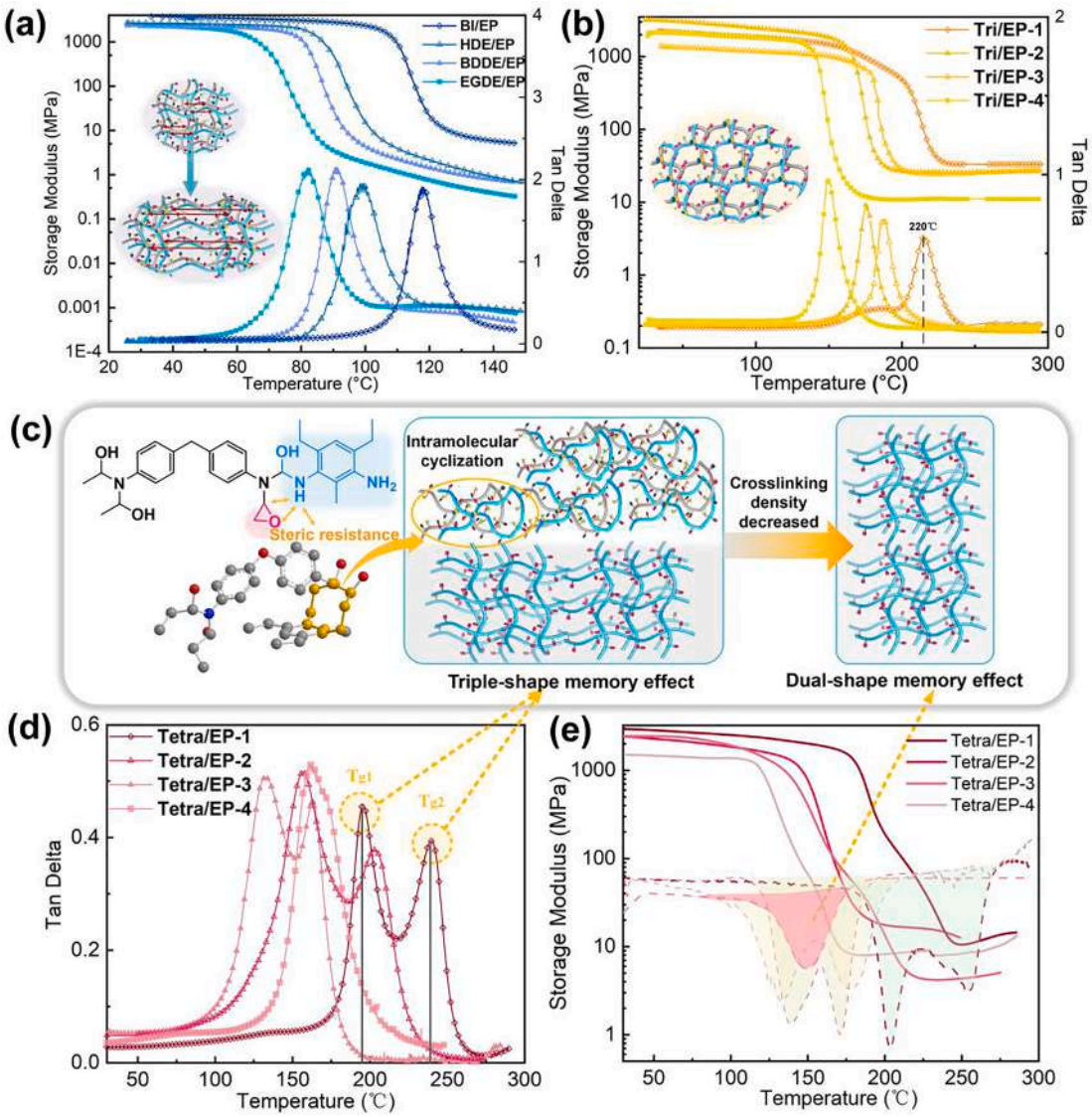

Fig. 3. DMA analysis of SMEPs with different cross-linked network structures. (a) DMA curve of Bi-EP system and its molecular diagram. (b) DMA curve of Tri-EP system and its molecular diagram. (c) The mechanism of Tetra-EP system ring internalization and the schematic diagram of its intersection network structure. (d) Loss factor curve of DMA test of Tetra-EP system. (e) Modulus and differential curve of DMA test of Tetra-EP system.

temperature also increases to 400 °C. This is attributed to the increased number of benzene rings, which improves the thermal stability of the structure.

3.3. Thermomechanical behavior

From the DMA results presented in Fig. 3a, the presence of longer alkyl chains increases the flexibility of the molecular system, leading to a gradual decrease in Tg. Trifunctional epoxy monomers did not undergo intramolecular cyclization because of moderate molecular steric hindrance, and consequently, they reacted gradually reacted with the polyamines to form a hyperbranched structure crosslinked network. The presence of a single DMA peak indicates that the intramolecular cyclization side reaction is closely related to the crosslinking density, as evidenced by Fig. 3b, wherein Tri/EP-1 exhibits a higher T_g (220 °C) than Tetra/EP-1. We choose multiple reaction sites, which means that with multiple active hydrogen curing agents (DETDA), active hydrogen in primary amine reacts with epoxy group to generate secondary amine, and active hydrogen in secondary amine further reacts with epoxy group to generate tertiary amine. It further promotes the close arrangement of cross-linked network structures. Owing to the intramolecular cyclization side reaction caused by the steric hindrance effect, the cross-linking reaction generates different network structures in situ, as shown in Fig. 3c. Additionally, Fig. 3d shows the DMA test curves obtained for the Tetra-EP systems, wherein two separated peaks are present in the loss angle tangent curves of the various samples, except for Tetra/EP-4, Based on these observations, it was considered that intermolecular crosslinking and the formation of a non-crosslinked inner ring could potentially occur during the curing reaction [35]. Once one of the four epoxy groups reacted, the steric hindrance made it difficult for the adjacent epoxy groups to react with the other amino groups of the amine-curing agent. Attias et al. reported that ~65 % of the epoxy groups in the glycidyl amine type epoxy resin (TGDDM)/Diamino diphenyl sulfone (DDS) system will participate in the cyclization side reaction of cyclization [36]. The possibility of intramolecular cyclization is increased during the epoxy closed-loop process. Due to the close distance between the two substituent groups, the steric hindrance makes it difficult for the other epoxy group to react with the active hydrogen on other molecules, so it is forced to choose the active hydrogen on the same curing agent to continue the reaction. There are many factors influencing intramolecular cyclization, among which steric hindrance is the most important. Secondly, the greater the viscosity of the curing

system, the greater the probability of cyclization reaction. However, when the length of alkyl carbon chain is short, intramolecular cyclization cannot occur [37,38]. It has also been proved that the cyclization effect can be effectively avoided by slowly dropping monomers [39]. The low hindrance to the reaction with the hydroxyl groups and secondary amines of the reacted molecules made that epoxy group susceptible to intramolecular cyclization. Further, the tetra-functional system had a higher crosslink density. Furthermore, the less the crosslinking density of the tetra-functionality system leads to reduced steric resistance becomes as the crosslinking network density decreases, and the intramolecular cyclization side reaction does not occur. This accounts for the gradual change in the FT-IR spectrum from a single peak secondary amine to two primary amine peaks.

Similarly, two peaks are apparent in the differential curve of the storage modulus, suggesting two steps in the change in the storage modulus (Fig. 3e). For example, for Tetra/EP-1, the first and second transition peaks appeared at 190 °C (T_{g1}) and near 250 °C (T_{g2}), respectively. This can be explained considering that when the degree of crosslinking of tetra-functional epoxy monomers decreases, the curing reaction occurs to generate short chains, leading to an uneven distribution of network segments is uneven. Therefore, the peak width of the loss factor of the Tetra/EP-4 loss factor becomes larger. However, the appearance of multiple loss factor peaks suggests existing within the molecular network, in addition to two T_g values. Therefore, it can be inferred that the polyfunctional epoxy resin exhibited a TSME. As the degree of crosslinking increased, the original low T_g peak gradually shifted to the right. Importantly, we achieved simple in situ generation of SMEP with triple shape memory effect by molecular network structure design.

3.4. Super-tough behavior

The mechanical properties of polymers play a crucial role in determining their potential applications. Fig. 4a shows a molecular schematic of the Bi-EP system. The synergistic effect of flexible chains and hydrogen bonds results in record mechanical super stretchability and deformation behavior. At the same degree of crosslinking, longer alkyl chains are associated with a higher flexibility of the molecular chains in the system, and thus easier slipping of molecular chains during stretching and higher elongation at the break. Fig. 4b shows the

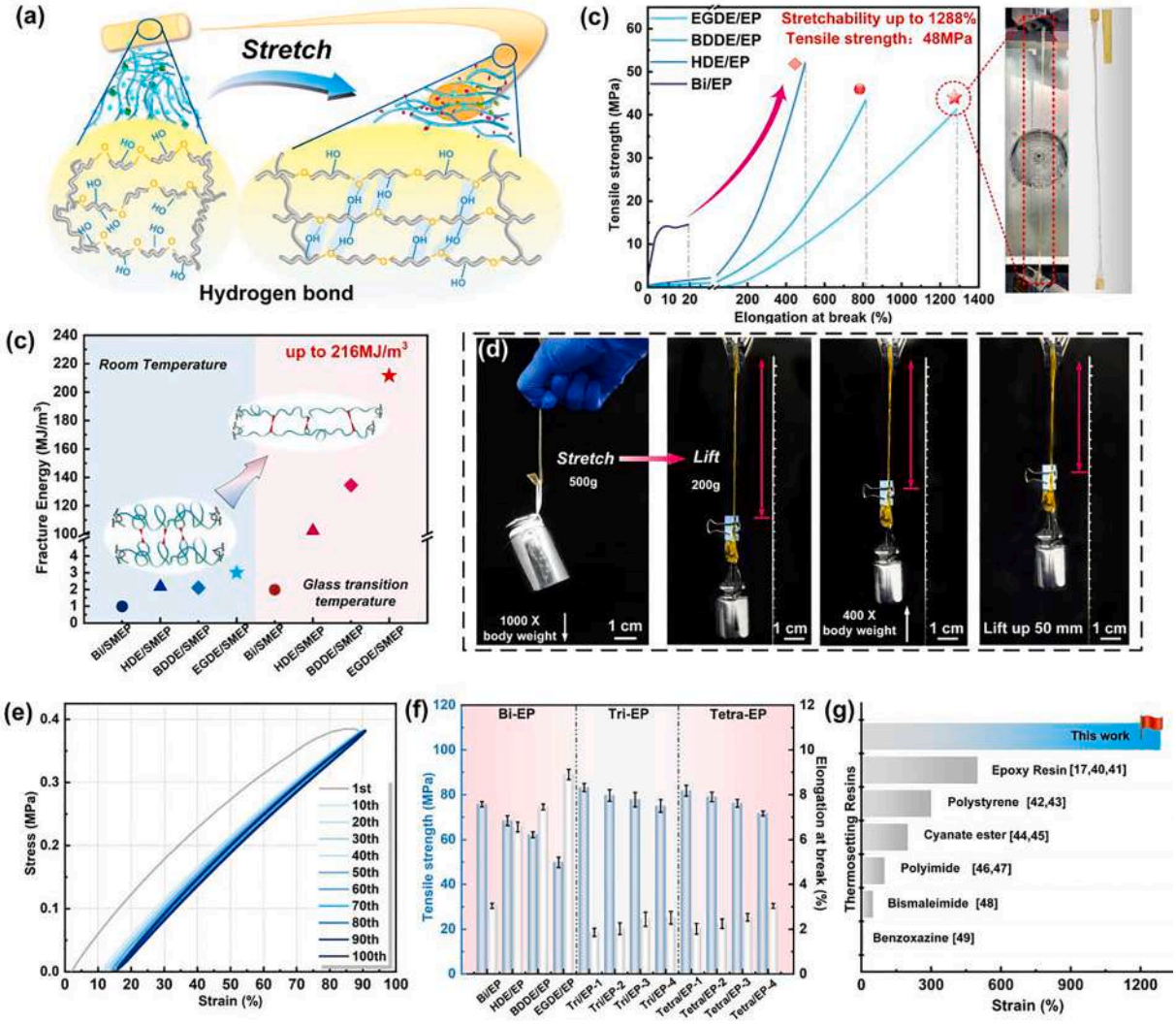

Fig. 4. Mechanical properties of SMEPs with different crosslinked network structures. (a) Molecular schematic diagram of the mechanism of the synergistic toughening of hydrogen bond and flexible chain in Bi-EP system. (b) Tensile stress–strain curves of Bi-EP systems at Tg. (c) The fracture energy of Bi-EP system was calculated at room temperature and Tg, respectively. (d) The 500 g weight is hung on the EDGE/SMEP, then the 200 g weight is replaced and lifted 5 cm under the recovery driving force, the scale bar is 1 cm in length. (e) Bi/EP-4 undergoes 100 tension load/unload cycles and set a stress–strain curve under 90 % tension strain. (f) Fracture elongation and tensile strength of all samples at room temperature. (g) Our work studies the tensile properties of SMEP, compared with other reports [17,40–49].

stress–strain curves of the Bi-EP system measured at Tg. Evidently, the Bi-EP tensile properties improved appreciably at high temperatures. The stretched states were recorded and compared. Analysis results of the tensile curves of the remaining samples at room temperature reveal that high functionality could markedly improve the strength of the material (Fig. S5). The hydroxyl groups (formed from the ring opening of epoxy groups) and the ether bonds collectively formed hydrogen bonds, imparting exceptional fracture toughness (1288 %) to the network structure. As a result, the thermosetting epoxy network maintained high strength up to 48 MPa even at high temperatures, resulting in increased stretchability and delayed fracture. Fig. 4c shows the fracture energy of Bi-EP system at room and high temperatures calculated from the stress–strain curves. Notably, this cooperative mechanism imparts the SMEP with high fracture toughness (216 MJ/m^3) and high strength (>40 MPa), while avoiding the tradeoff between toughness and stiffness. However, the fracture energy gradually decreased as the toughening effect strengthened. The sample could be naturally stretched to 12 cm when bearing a weight of 500 g (100 × the specimen weight) at 100 °C. The replacement of the 500 g weights with 200 g weights raised the weights by 50 mm. Subsequently, after the recovery of the driving force and weight balancing, no further upward recovery is observed, and the equilibrium state is reached (Fig. 4d), see video S1.

Fig. 4e shows the constant-temperature tensile cyclic stretch–recovery curves, wherein the EGDE/EP was subjected to 100 loading/unloading cycles at 90 °C using a deformation rate of 90 %. After the first loading/unloading cycle, the residual deformation was 6 %, which increased further to 8 % after 100 loading/unloading cycles. Significant agreement was noted between the deformation curves observed during cycling, suggesting that the system exhibited an exceptional and stable shape memory performance, in addition to excellent fatigue resistance. Furthermore, Fig. 4f shows a comprehensive comparison of the mechanical properties of all the samples at room temperature. The Tri-EP and Tetra-EP samples exhibited high tensile strength, suggesting that polyfunctionality appreciably increased system strength, accompanied by a decrease in fracture properties. As shown in Fig. S6, while being heated to a high temperature, a sample was stretched and wound to a length of more than 14 cm, while maintaining its original shape was maintained. At T_g, the sample rapidly recovered to its original state (See video S2). Importantly, this system exhibited the highest tensile toughness and strength of all epoxy resins reported to

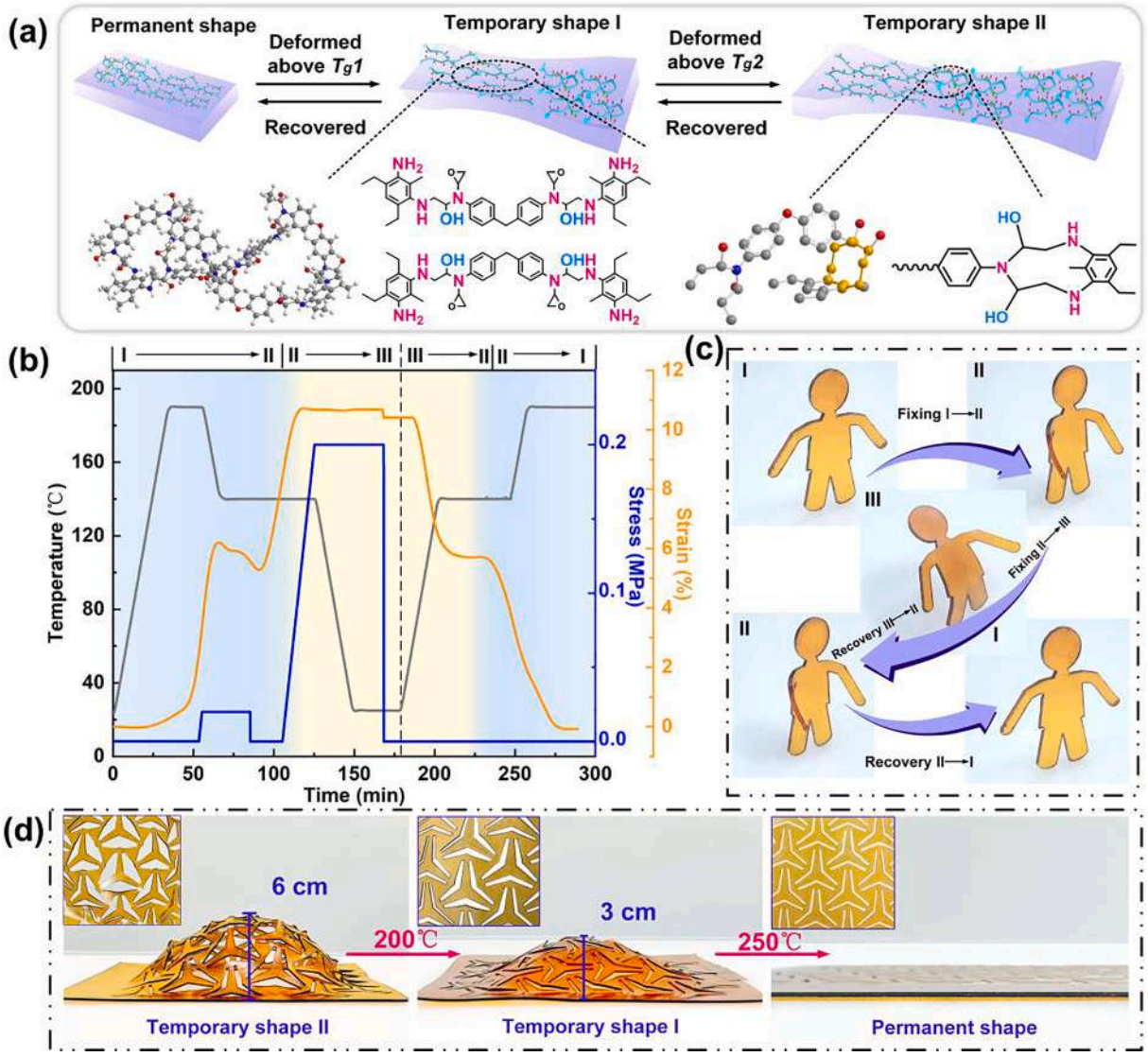

Fig. 5. Triple shape memory performance of Tetra-EP system. (a) Triple-shape memory mechanism maps of different intersecting networks were generated in situ due to ring internalization. (b) The DMA curve of the Tetra/EP-2 was shaped at different temperatures and replied to one by one. (c) The "triple statue" formed by the triple shape memory successively stretches out its hands and bends down. (d) Tetra/EP-1 was fabricated as a superstructure for topological deformation to achieve multilevel deformation expansion, which decreased from 6 cm height of temporary shape II state to 3 cm final shape recovery of temporary shape I state.

date, extremely strong resins are still highly reliable and durable. With the increase of cross-linking density, the number of cross-linking bonds in unit volume increases, reflecting that the cross-linking network structure is more compact, the heat resistance of the resin is improved, and the tensile strength is increased. These cooperative mechanisms endow self-sensing SMEP with high fracture toughness and high Young's modulus, avoiding the tradeoff between toughness and stiffness. We compare the tensile properties of this work with other thermosetting resins, and the deformation of SMEP has far exceeded that of other thermosetting resins reported so far [17,40–49]. Therefore, this study paves the way for the application of such SMPs in diverse engineering fields that require unprecedented mechanical properties of SMPs (Fig. 4g).

3.5. Triple-shape memory behavior

Highly functional epoxy resins are susceptible to intramolecular cyclization due to steric hindrance and therefore exhibit a satisfactory TSME, as shown in Fig. 5a. Importantly, triple-shape memory properties can be combined with superstructural topological deformation to achieve multi-stage deformation and unfolding, which playing key roles in fields such as aerospace industry. Fig. 5b shows the quantitative TSME results for the Tetra/EP-2 system, which were evaluated using external forces of 0.02 MPa and 0.2 MPa were used to stretch and shape at 190 °C and 150 °C respectively. The temporary shape that was fixed at 190 °C was formed by the movement of the chain segments movement at low transition temperature, resulting in a certain degree of recovery during shaping at 150 °C. This is because the mobility of molecular chains had significantly higher at high transition temperatures, leading to excellent deformability and shape fixation are excellent. Therefore, smart, programmable, and reconfigurable materials can be developed based on multiple deformation cycles and high-temperature-resistance, lightweight, high-strength, deformable, and high-performance smart materials because of their responses to different temperatures. A mobile "triple figurine" was prepared. During the first shaping process, the hands of the figurine were extended forward at 150 °C. During the second shaping process, the figurine was shaped by bending it backward at 190 °C. As the temperature increased from 150 °C to 190 °C, the figurine gradually recovered from temporary shape II state to temporary shape I state and eventually recovered to its original state (Fig. 5c). These results indicate that smart deployable devices with complex structures can be rapidly and easily constructed using the material's excellent TSME. As shown in Fig. 5d, the active deformation and geometric topological composition of an SMP were combined to form a tunable material with high deformability. Specifically, Tetra/EP-1 was shaped at each of its two T_g values such that it protruded to a height of 3 cm and 6 cm, respectively. The planar cellular structure structures are shown in the upper left figure, where the deformation of temporary shape II state stretched the edges of the cellular structure to straight lines. After the material gradually recovered from temporary shape II state at 200 °C to temporary shape I state, which was subsequently maintained for 1 min, and subsequently, the temperature was increased to 250 °C, causing the material to recover to its original shape from temporary shape I state. Thus, a multi-stage 3D-to-2D transformation process is achieved (see video S3), and this material could carry more than 20 times its weight (500 g) when fully stretched (temporary shape II), as shown in Fig. S7.

4. Application potential of SMEPs

Owing to its excellent super stretching properties, Bi-EP appears suitable for application in wearable electronic devices, artificial muscles, strain monitoring, and stretchable devices. Using self-sensing characteristics of SMP to achieve various shape deformations and functions provides application potential for the manufacture of artificial muscles that are required to undergo large deformations and to form multiple shapes (Fig. 6a). Therefore, it was demonstrated that a deformation from 150° to 90° was completed, and the application of SMEP in artificial muscle was preliminarily verified. In this study, EDGE/SMEP was prepared to achieve stretchability. Based on 100 cycles tensile test cycles were performed to demonstrate the excellent fatigue resistance of EDGE/SMEP. Owing to its high-temperature resistance and self-sensing characteristics, Tri-EP system should be applicable in lock release mechanisms. Spatial lock release mechanism primarily comprises a conventional mechanical pyrotechnic device. However, this structure has many disadvantages, such as shock caused by violent vibrations during release, large mass, and lack of reusability. Therefore, the replacement of conventional pyrotechnic devices with SMPs with unique variable stiffness properties has emerged as a key research focus. Fig. 6b shows a combined system composed of a lock–release mechanism (mimicking the layers of a lotus flower) and a high-temperature-resistant SMEP. This system is capable of releasing layer by layer. The entire release process is slow and orderly, as shown in video S5.

As single dual-SMPs can no longer meet the requirements of this process, multiple-SMPs must be employed. Considering satellite applications, different satellites in preset orbits will possess different orbit entry methods and processes, such as transitional orbit entry. Specifically, at the point when the satellite is deployed in the parking orbit [50]. At this time, the solar panel is not deployed (I state), as shown in Fig. 6c. Subsequently, in low-drag configuration, the solar panels begin to expand but do not need to be fully extended and are parallel to the ground (II state). When satellites are ignited and lifted to the operational orbit, they will readjust their attitude and hardware such that the antenna faces the Earth. At this time, the solar array is required to be fully deployed and perpendicular to the sun (III state). Therefore, upon simulating this satellite orbit entry mode. When the solar array is heated to 200 °C, it gradually transits from temporary shape II to temporary shape I (Fig. S8). When the satellite is heated to 200 °C by electric heating film, the satellite gradually transits from temporary shape II to temporary shape (see video S4). Subsequently, as the voltage rises from 3.2 to 4.2 V, the temperature rises to 250 °C, and the heating temperature of the sample gradually increases to complete the action of expanding from temporary shape II state to temporary shape I state and finally returning to the original state At this point, the satellite is fully deployed. Compared with the reported comprehensive properties of thermosetting resins, our study represents a breakthrough in terms of both the tensile strain and heat resistance properties, as compared with Fig. 6d.

5. Conclusion

In this study, a programmable SMEP system was developed. SMEPs with tunable properties were produced using a range of epoxy monomers via topological structure cross-linking networks. The mechanism by which the microscopic polyfunctional network structure affects macroscopic properties was revealed through MD simulations. In particular, the introduction of a dual synergistic effect of flexible chains and hydrogen bonds resulted in an epoxy resin that exhibited an unprecedented ultra-high toughness of up to 1288 % and high reliability during nearly 100 tensile recovery cycles. The compactly arranged crosslinked network structure of high-functional SMEPs led to considerably higher T_g values (greater than200 °C) than those of previously reported epoxy resins. Significantly triple-SMEPs with different network structures were formed via an intramolecular cyclization through steric hindrance effect. Overall, this study provides the foundation for preparing new-generation materials with high toughness and stiffness properties. Moreover, triple-SMEPs designed for the multi-stage unfolding strategy required by the aerospace industry will be expected to inspire future research and applications.

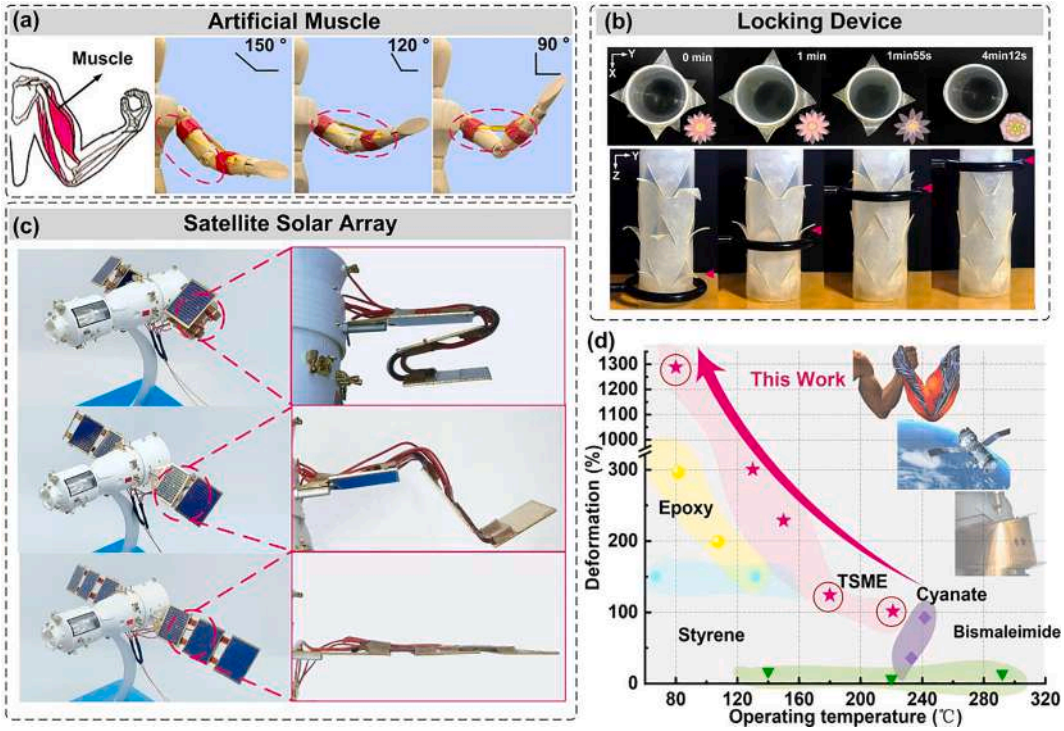

Fig. 6. Application verification of SMEPs with different cross-linked network structures. (a) EDGE/SMEP samples exhibiting stretching and shape recovery, ultimately mimicking the lifting behavior exhibited by an artificial muscle. (b) Layer-by-layer locking structure of Tri/EP-1 imitated the "lotus" structure and gradually closed up under 240 °C heating (c) Tetra/EP-1 with TSME drives the completion of two phases of satellite solar wing expansion at different temperatures. (d) The breakthrough progress made in the current work is compared with the comprehensive performance of other thermosetting resins reported.

Declaration of Competing Interest

The authors declare that they have no known competing financial interests or personal relationships that could have appeared to influence the work reported in this paper.

Data availability

Data will be made available on request.

Acknowledgments

We give thanks to the National Key R&D Program of China (2022YFB3805700).

Appendix A. Supplementary data

Supplementary data to this article can be found online at https://doi.org/10.1016/j.cej.2023.141282.

References

[1] J. Leng, X. Lan, Y. Liu, S. Du, Shape-memory polymers and their composites: Stimulus methods and applications, Prog. Mater Sci. 56 (7) (2011) 1077–1135, https://doi.org/10.1016/j.pmatsci.2011.03.001.
[2] C. Liu, H. Qin, P.T. Mather, Review of progress in shape-memory polymers, J. Mater. Chem. 17 (16) (2007) 1543–1558, https://doi.org/10.1039/b615954k.
[3] L. Luo, F. Zhang, J. Leng, Shape memory epoxy resin and its composites: from materials to applications, Research 2022 (2022) 1–25, https://doi.org/10.34133/2022/9767830.
[4] X. Pang, L. Qin, B.o. Xu, Q. Liu, Y. Yu, Ultralarge contraction directed by light-driven unlocking of prestored strain energy in linear liquid crystal polymer fibers, Adv. Funct. Mater. 30 (32) (2020), https://doi.org/10.1002/adfm.202002451.
[5] Y. Feng, M. Qin, H. Guo, K. Yoshino, W. Feng, Infrared-actuated recovery of polyurethane filled by reduced graphene oxide/carbon nanotube hybrids with high energy density, ACS Appl. Mater. Interfaces 5 (21) (2013) 10882–10888, https://doi.org/10.1021/am403071k.
[6] X. Pang, J.-a. Lv, C. Zhu, L. Qin, Y. Yu, Photodeformable azobenzene-containing liquid crystal polymers and soft actuators, Adv. Mater. 31 (52) (2019), https://doi.org/10.1002/adma.201904224.
[7] Y. Liu, W. Wu, J. Wei, Y. Yu, Visible light responsive liquid crystal polymers containing reactive moieties with good processability, ACS Appl. Mater. Interfaces 9 (1) (2017) 782–789, https://doi.org/10.1021/acsami.6b11550.
[8] C. Lin, J. Lv, Y. Li, F. Zhang, J. Li, Y. Liu, L. Liu, J. Leng, 4D-printed biodegradable and remotely controllable shape memory occlusion devices, Adv. Funct. Mater. 29 (51) (2019), https://doi.org/10.1002/adfm.201906569.
[9] Y. Wu, Y. Lin, Y. Zhou, F. Zuo, Z. Zheng, X. Ding, Light-induced shape memory polymer materials, Prog. Chem 24 (10) (2012) 2004–2010.
[10] W.M. Huang, B. Yang, Y. Zhao, Z. Ding, Thermo-moisture responsive polyurethane shape-memory polymer and composites: a review, J. Mater. Chem. A 20 (17) (2010) 3367–3381, https://doi.org/10.1039/b922943d.
[11] K. Yu, Z. Zhang, Y. Liu, J. Leng, Carbon nanotube chains in a shape memory polymer/carbon black composite: To significantly reduce the electrical resistivity, Appl. Phys. Lett. 98 (7) (2011) 074102.
[12] Z. Liu, Q. Li, W. Bian, X. Lan, Y. Liu, J. Leng, Preliminary test and analysis of an ultralight lenticular tube based on shape memory polymer composites, Compos. Struct. 223 (2019), https://doi.org/10.1016/j.compstruct.2019.110936.
[13] J. Ma, Y. Yang, C. Valenzuela, X. Zhang, L. Wang, W. Feng, Mechanochromic, shape-programmable and self-healable cholesteric liquid crystal elastomers enabled by dynamic covalent boronic ester bonds, Angew. Chem. Int. Ed. 61(9) (2022). doi: 10.1002/anie.202116219.
[14] G. Chen, B. Jin, Y. Shi, Q. Zhao, Y. Shen, T. Xie, Rapidly and repeatedly reprogrammable liquid crystalline elastomer via a shape memory mechanism, Adv. Mater. 34 (21) (2022), https://doi.org/10.1002/adma.202201679.
[15] J. Sun, B.o. Peng, Y. Lu, X. Zhang, J. Wei, C. Zhu, Y. Yu, A photoorganizable triple shape memory polymer for deployable devices, Small 18 (9) (2022), https://doi.org/10.1002/smll.202106443.
[16] Z. Li, Y. Yang, L. Ma, H. Liu, X. Zhang, Shape memory epoxy resin and its composite with good shape memory performance and high mechanical strength, Polym. Bull. (2022), https://doi.org/10.1007/s00289-022-04140-2.
[17] N. Zheng, G. Fang, Z. Cao, Q. Zhao, T. Xie, High strain epoxy shape memory polymer, Polym. Chem. 6 (16) (2015) 3046–3053, https://doi.org/10.1039/c5py00172b.
[18] L. Luo, F. Zhang, W. Pan, Y. Yao, Y. Liu, J. Leng, Shape memory polymer foam: active deformation, simulation and validation of space environment, Smart Mater. Struct. 31 (3) (2022) 035008, https://doi.org/10.1088/1361-665X/ac4ba8.
[19] X. Lan, L. Liu, C. Pan, F. Li, Z. Liu, G. Hou, J. Sun, W. Dai, L. Wang, H. Yue, Y. Liu, J. Leng, X. Zhong, Y. Tang, Smart solar array consisting of shape-memory releasing mechanisms and deployable hinges, AIAA J. 59 (6) (2021) 2200–2213, https://doi.org/10.2514/1.J059281.

[20] X. Lan, L. Liu, F. Zhang, Z. Liu, L. Wang, Q. Li, F. Peng, S. Hao, W. Dai, X. Wan, Y. Tang, M. Wang, Y. Hao, Y. Yang, C. Yang, Y. Liu, J. Leng, World's first spaceflight on-orbit demonstration of a flexible solar array system based on shape memory polymer composites, Sci. China-Technol. Sci. 63 (8) (2020) 1436–1451, https://doi.org/10.1007/s11431-020-1681-0.
[21] M. Behl, I. Bellin, S. Kelch, W. Wagermaier, A. Lendlein, Dual and Triple Shape capability of AB polymer networks based on poly(epsilon-caprolactone) dimethacrylates, in: Symposium on Advances in Material Design for Regenerative Medicine, Drug Delivery and Targeting/Imaging held at the 2008 MRS Fall Meeting, Boston, MA, 2008, pp. 3-8.
[22] T. Xie, Tunable polymer multi-shape memory effect, Nature 464 (7286) (2010) 267–270, https://doi.org/10.1038/nature08863.
[23] Z. Li, J. Hu, L.i. Ma, H. Liu, High glass transition temperature shape-memory materials: Hydroxyl-terminated polydimethylsiloxane-modified cyanate ester, J. Appl. Polym. Sci. 137 (18) (2020), https://doi.org/10.1002/app.48641.
[24] M. Fejos, K. Molnar, J. Karger-Kocsis, Epoxy/polycaprolactone systems with triple-shape memory effect: electrospun nanoweb with and without graphene versus co-continuous morphology, Materials 6 (10) (2013) 4489–4504, https://doi.org/10.3390/ma6104489.
[25] S.-K. Ahn, R.M. Kasi, Exploiting microphase-separated morphologies of side-chain liquid crystalline polymer networks for triple shape memory properties, Adv. Funct. Mater. 21 (23) (2011) 4543–4549, https://doi.org/10.1002/adfm.201101369.
[26] T. Xie, X. Xiao, Y.-T. Cheng, Revealing triple-shape memory effect by polymer bilayers, Macromol Rapid Commun. 30 (21) (2009) 1823–1827, https://doi.org/10.1002/marc.200900409.
[27] L. Luo, F. Zhang, J. Leng, Multi-performance shape memory epoxy resins and their composites with narrow transition temperature range, Compos. Sci. Technol. 213 (2021), https://doi.org/10.1016/j.compscitech.2021.108899.
[28] L. Wang, F. Zhang, Y. Liu, S. Du, J. Leng, Photosensitive composite inks for digital light processing four-dimensional printing of shape memory capture devices, ACS Appl. Mater. Interfaces 13 (15) (2021) 18110–18119, https://doi.org/10.1021/acsami.1c02624.
[29] M. Zhong, R. Wang, K. Kawamoto, B.D. Olsen, J.A. Johnson, Quantifying the impact of molecular defects on polymer network elasticity, Science 353 (6305) (2016) 1264–1268, https://doi.org/10.1126/science.aag0184.
[30] W. Zihan, K. Peibin, W.u. Tianyu, C. Dongli, Y. Xiaoping, S. Gang, Atomistic understanding of cross-linking network in different epoxy resin: Effect of loop structure, Polymer 243 (2022), https://doi.org/10.1016/j.polymer.2022.124629.
[31] V. Bellenger, J. Verdu, J. Francillette, P. Hoarau, E. Morel, Infrared study of hydrogen-bonding in amine-cross-linked epoxies, Polymer 28 (7) (1987) 1079–1086, https://doi.org/10.1016/0032-3861(87)90246-1.
[32] H. Yamasaki, S. Morita, Two-step curing reaction of epoxy resin studied by thermal analysis and infrared spectroscopy, Appl. Spectrosc. 66 (8) (2012) 926–933, https://doi.org/10.1366/11-06437.
[33] Y. Gu, K. Kawamoto, M. Zhong, M. Chen, M.J.A. Hore, A.M. Jordan, L.T.J. Korley, B.D. Olsen, J.A. Johnson, Semibatch monomer addition as a general method to tune and enhance the mechanics of polymer networks via loop-defect control, Proc. Natl. Acad. Sci. U.S.A. 114 (19) (2017) 4875–4880, https://doi.org/10.1073/pnas.1620985114.
[34] C.G. Gong, J. Miravet, J.M.J. Frechet, Intramolecular cyclization in the polymerization of AB(x) monomers: Approaches to the control of molecular weight and polydispersity in hyperbranched poly(siloxysilane), J. Polym. Sci. Part A-Polym. Chem. 37 (16) (1999) 3193–3201, https://doi.org/10.1002/(sici)1099-0518(19990815)37:16.
[35] A.J. Attias, J. Ancelle, B. Bloch, F. Laupretre, chemical-structure of networks resulting from curing of n, n-diglycidylaniline-type resins with aromatic-amines. 2. Detection and characterization of intermolecular etherification on model compounds, J. Polym. Sci. A: Polym. Chem. 28 (7) (1990) 1661–1679, https://doi.org/10.1002/pola.1990.080280702.
[36] A.J. Attias, B. Bloch, F. Laupretre, Chemical-structure of networks resulting from curing of N,N-diglycidylaniline-type resins with aromatic-amines. 4. Characterization of TGDDM DDS and TGDDM DDM networks by high-resolution solid-state C-13-NMR, J. Polym. Sci. A: Polym. Chem. 28 (1990) 3445–3466.
[37] V. Percec, M. Kawasumi, liquid-crystalline polyethers based on conformational isomerism. 23. Synthesis and characterization of a thermotropic nematic liquid-crystalline dendrimeric polymer, Macromolecules 25 (15) (1992) 3843–3850, https://doi.org/10.1021/ma00041a004.
[38] T. Liu, X. Miao, X. Geng, A. Xing, L. Zhang, Y. Meng, X. Li, Control-synthesized multilayer hyperbranched-hyperbranched polyethers with a tunable molecular weight and an invariant degree of branching, New J. Chem. 40 (4) (2016) 3432–3439, https://doi.org/10.1039/c5nj02895g.
[39] A. Mock, A. Burgath, R. Hanselmann, H. Frey, Synthesis of hyperbranched aromatic homo- and copolyesters via the slow monomer addition method, Macromolecules 34 (22) (2001) 7692–7698, https://doi.org/10.1021/ma000515a.
[40] T. Xie, I.A. Rousseau, Facile tailoring of thermal transition temperatures of epoxy shape memory polymers, Polymer 50 (8) (2009) 1852–1856, https://doi.org/10.1016/j.polymer.2009.02.035.
[41] A.B. Leonardi, L.A. Fasce, I.A. Zucchi, C.E. Hoppe, E.R. Soule, C.J. Perez, R.J. J. Williams, Shape memory epoxies based on networks with chemical and physical crosslinks, Eur. Polym. J. 47 (3) (2011) 362–369, https://doi.org/10.1016/j.eurpolymj.2010.12.009.
[42] F. Xie, L. Huang, J. Leng, Y. Liu, Thermoset shape memory polymers and their composites, J. Intell. Mater. Syst. Struct. 27 (18) (2016) 2433–2455, https://doi.org/10.1177/1045389x16634211.
[43] G.P. Tandon, K. Goecke, K. Cable, J. Baur, Durability assessment of styrene- and epoxy-based shape-memory polymer resins, J. Intell. Mater. Syst. Struct. 20 (17) (2009) 2127–2143, https://doi.org/10.1177/1045389x09348255.
[44] R. Biju, C.P.R. Nair, Effect of phenol end functional switching segments on the shape memory properties of epoxy-cyanate ester system, J. Appl. Polym. Sci. 131 (23) (2014).
[45] Y. Zhao, D. Zhang, L. Guo, Shape-memory behavior of bisphenol A-type cyanate ester/carboxyl-terminated liquid nitrile rubber coreacted system, Colloid. Polym. Sci. 292 (10) (2014) 2707–2713, https://doi.org/10.1007/s00396-014-3321-x.
[46] X. Xiao, D. Kong, X. Qiu, W. Zhang, F. Zhang, L. Liu, Y. Liu, S. Zhang, Y. Hu, J. Leng, Shape-memory polymers with adjustable high glass transition temperatures, Macromolecules 48 (11) (2015) 3582–3589, https://doi.org/10.1021/acs.macromol.5b00654.
[47] X. Xiao, D. Kong, X. Qiu, W. Zhang, Y. Liu, S. Zhang, F. Zhang, Y. Hu, J. Leng, Shape memory polymers with high and low temperature resistant properties, Sci. Rep. 5 (2015), https://doi.org/10.1038/srep14137.
[48] Q. Zhang, H. Wei, Y. Liu, J. Leng, S. Du, Triple-shape memory effects of bismaleimide based thermosetting polymer networks prepared via heterogeneous crosslinking structures, RSC Adv. 6 (13) (2016) 10233–10241, https://doi.org/10.1039/c5ra24247a.
[49] H. Schaefer, A. Hartwig, K. Koschek, The nature of bonding matters: Benzoxazine based shape memory polymers, Polymer 135 (2018) 285–294, https://doi.org/10.1016/j.polymer.2017.12.029.
[50] R.D. Fleeter, Method of deploying payload satellite into predetermined low-earth orbit, includes deploying payload satellite into geo-synchronous- transfer orbit from geo-synchronous-transfer launch vehicle, AERO ASTRO INC, US6286787, 2001.